# bSUM: A bead-supported unilamellar membrane system facilitating unidirectional insertion of membrane proteins into giant vesicles

Hui Zheng,[1,2*] Sungsoo Lee,[1,3*] Marc C. Llaguno[1,4], and Qiu-Xing Jiang[1,5]

[1]Department of Cell Biology, [2]Department of Physiology, and [3]Department of Biophysics, The University of Texas Southwestern Medical Center, Dallas, TX 75390

[4]Department of Cell Biology, Yale University, New Haven, CT 06510

[5]Department of Microbiology and Cell Science, University of Florida, Gainesville, FL 32611

Fused or giant vesicles, planar lipid bilayers, a droplet membrane system, and planar-supported membranes have been developed to incorporate membrane proteins for the electrical and biophysical analysis of such proteins or the bilayer properties. However, it remains difficult to incorporate membrane proteins, including ion channels, into reconstituted membrane systems that allow easy control of operational dimensions, incorporation orientation of the membrane proteins, and lipid composition of membranes. Here, using a newly developed chemical engineering procedure, we report on a bead-supported unilamellar membrane (bSUM) system that allows good control over membrane dimension, protein orientation, and lipid composition. Our new system uses specific ligands to facilitate the unidirectional incorporation of membrane proteins into lipid bilayers. Cryo–electron microscopic imaging demonstrates the unilamellar nature of the bSUMs. Electrical recordings from voltage-gated ion channels in bSUMs of varying diameters demonstrate the versatility of the new system. Using KvAP as a model system, we show that compared with other in vitro membrane systems, the bSUMs have the following advantages: (a) a major fraction of channels are orientated in a controlled way; (b) the channels mediate the formation of the lipid bilayer; (c) there is one and only one bilayer membrane on each bead; (d) the lipid composition can be controlled and the bSUM size is also under experimental control over a range of 0.2–20 µm; (e) the channel activity can be recorded by patch clamp using a planar electrode; and (f) the voltage-clamp speed (0.2–0.5 ms) of the bSUM on a planar electrode is fast, making it suitable to study ion channels with fast gating kinetics. Our observations suggest that the chemically engineered bSUMs afford a novel platform for studying lipid–protein interactions in membranes of varying lipid composition and may be useful for other applications, such as targeted delivery and single-molecule imaging.

The Journal of General Physiology

## INTRODUCTION

In the past, structural and functional studies of voltage-gated ion channels have provided profound insights into their function (Jiang et al., 2003; MacKinnon, 2003; Miller, 2003; Tombola et al., 2006, 2007; Long et al., 2007; Bezanilla, 2008; Villalba-Galea et al., 2009a,b; Catterall and Yarov-Yarovoy, 2010; Tao et al., 2010; DeCaen et al., 2011; Payandeh et al., 2011, 2012; Vargas et al., 2011; Catterall, 2012; Jiang and Gonen, 2012). Most of the past studies assumed that the lipids around voltage-gated ion channels act as a solvent for their hydrophobic transmembrane domains, whereas the proteinaceous parts are solely responsible for voltage-dependent function. Recent studies, however, recognize that lipids play critically important roles in the controlled opening or closing (gating) of these ion channels (Ramu et al., 2006; Schmidt et al., 2006; Schmidt and MacKinnon, 2008; Xu et al., 2008; Zheng et al., 2011; Jiang and Gonen, 2012; Brohawn et al., 2014; Hite et al., 2014). Compelling evidence from these studies suggests that lipids surrounding a voltage-gated potassium (Kv) channel exert strong gating effects on the channels by directly affecting the energetics behind the conformational changes of the voltage-sensor domains. We observed that removal of the phosphate groups in the lipid bilayers around a Kv channel directly switches its voltage-sensor domains into the "DOWN" (also called the "resting" or "hyperpolarized") conformation in the absence of any change in transmembrane electrostatic potential. We named this phenomenon the "lipid-dependent

*H. Zheng and S. Lee contributed equally to this paper.

Correspondence to Qiu-Xing Jiang: qiu-xing.jiang@utsouthwestern.edu or qxjiang@ufl.edu

M.C. Llaguno's present address is Dept. of Cell Biology, Yale University, New Haven, CT 06510.

Q.-X. Jiang's present address is Dept. of Microbiology and Cell Science, University of Florida, Gainesville, FL 32611.

Abbreviations used in this paper: AB-NTA, *N*-(5-amino-1-carboxypentyl) iminodiacetic acid; BLM, bilayer lipid membrane; bSUM, bead-supported unilamellar membrane; cryoEM, cryo–electron microscopy; EDC, 1-ethyl-3-(3-dimethyl-aminopropyl) carbodiimide hydrochloride; Fv, a variable fragment of the 33H1 antibody; GFP, green fluorescent protein; Kv, voltage-gated potassium; MTS-PEG5K, methoxy-poly-(ethylene glycol)-5000 amido-proprionyl methanethiosulfonate; Sulfo-NHS, *N*-hydroxysulfosuccinimide.



The Rockefeller University Press $30.00
J. Gen. Physiol. Vol. 147 No. 1 77–93
www.jgp.org/cgi/doi/10.1085/jgp.201511448

gating" effect (Schmidt et al., 2006; Zheng et al., 2011) to reflect the slower steady-state changes in the gating property of a channel. These studies suggest that many of the lipid molecules in eukaryotic cell membranes, which lack phosphate groups in their headgroup regions, for example, cholesterol, may exert specific gating effects on voltage-gated ion channels using a similar mechanism.

Indeed, in eukaryotic cells, several mammalian voltage-gated ion channels have been reported to be localized in cholesterol-enriched microdomains (Martens et al., 2004). Treating cells with chemical reagents to manipulate the cholesterol content of plasma membranes resulted in significant changes in channel activity (Martens et al., 2000; Hajdú et al., 2003; Xia et al., 2004, 2008; Tóth et al., 2009). The observed effects varied from one channel to another and were found to be stimulatory by some and inhibitory by others, depending on the experimental conditions, the channels, and the cells. In certain cases, cholesterol was proposed to compete against PIP2 (or other phospholipids in a broader sense) for lipid-binding sites that are thought to be necessary for energetic coupling between the voltage-sensor domains and the pore domain (Chun et al., 2010, 2013; Zaydman et al., 2013, 2014; Coyan et al., 2014; Zaydman and Cui, 2014). How cholesterol or other lipids affect the voltage-gated ion channels and whether there is a unifying principle behind the lipid-dependent gating effects remain poorly understood.

Taking a broader view, there has been very limited understanding of how other non-phospholipids, such as glycolipids, gangliosides, etc., can affect voltage-gated channels that happen to be in an environment enriched with these lipids. One of the reasons for the current limitations and complexity is that electrical recordings from cell-attached patches or whole-cell membranes are not sufficient to define a causal relationship between changes in lipid composition and alterations in channel function, as a result of the strong heterogeneity in terms of lipid composition and organization in eukaryotic cell membranes. At a more fundamental level, how different lipid molecules may alter the activity of specific voltage-gated ion channels remains poorly understood. On the other hand, the altered cellular content of specific lipids, such as gangliosides, cholesterol, etc., was associated with changes in neuronal excitability and memory in animal models and tightly linked to neurological diseases, such as seizure, epilepsy, neurodegenerative diseases, etc. (Saini et al., 2004; Abi-Char et al., 2007; Guo et al., 2008; Wang and Schreurs, 2010; Pristerà et al., 2012). It is conceivable that a quantitative understanding of the gating effects exerted by various different non-phospholipids on voltage-gated ion channels would be important in revealing the molecular mechanisms responsible for these clinical observations, as well as the physico-chemical principles underlying lipid–channel interaction.

To quantitatively study the lipid–protein interactions that dictate the lipid-dependent gating effects on voltage-gated ion channels, we would be helped by a membrane system that allows for the finer manipulation of both the channel proteins and the lipids and is amenable to electrical recordings of macroscopic currents and single-channel events. We tested some of the tools available for analyzing lipid–protein interaction in bilayers that mimic eukaryotic membranes and experienced significant difficulties in controlling protein incorporation direction and lipid composition. Also, direct recordings from cell membranes, fused vesicles made of multilamellar membranes, planar bilayer membranes, solid-supported membranes, (functional) tethered lipid bilayers, droplet bilayer membranes, etc., suffered from limitations because of the heterogeneity of the lipids, organic solvents in the membranes, poor efficiency in protein incorporation, limited control over the directionality of protein insertion, and/or insufficient control over membrane fusion (Cohen et al., 1984; Atanasov et al., 2005; Bayley et al., 2008; Schulz et al., 2009; Finol-Urdaneta et al., 2010; Aimon et al., 2011; Iscla et al., 2011). We therefore need a new system.

Previously, we found that introducing 5–10% (weight ratio) cholesterol into decane-based planar lipid membranes (bilayer lipid membranes [BLMs]) made it fairly difficult to fuse channel-containing vesicles. We were not able to record channel activity well (Zheng et al., 2011). Similarly, we experienced difficulty in introducing sphingolipids into solvent-based BLMs and found that 1,2-dioleoyl-*sn*-glycero-3-phosphocholine (DOPC) or 1-palmitoyl-2-oleoyl-*sn*-glycero-3-phosphocholine (POPC) in decane forms a sticky gel-like phase over time, probably caused by trace amounts of water. Additionally, the solvent-based BLMs have a significant amount of solvent (decane or squalene, for example), which may alter the physicochemical properties of the bilayers, especially phase separation, interactions between neutral lipids (such as cholesterol), and the islands of solvent molecules in membranes composed of composite lipids (Needham et al., 1988; Lee et al., 2013). To overcome many of these technical limitations, we developed a chemical procedure to generate a new bead-supported unilamellar membrane (bSUM) system. In this system, a high density of carboxylate groups was first introduced onto the surfaces of beads that vary from 0.2 to 20 µm in diameter. These reactive carboxylates allowed the covalent linkage of bioactive ligands (Llaguno et al., 2014). Interactions with the chemically immobilized ligands attracted a high density of membrane proteins to the bead surface. These proteins were found to be able to support the reconstitution of a continuous bilayer around each bead. Such a membrane would allow the control of lipid composition and the predefined orientation of protein incorporation in membranes. It will enable us to quantitatively

define the effects of various natural lipid molecules in eukaryotic cell membranes on voltage-gated ion channels in a relatively homogeneous lipid environment.

## MATERIALS AND METHODS

### Materials

Two groups of silica beads of 0.20 and 5–20 µm in diameter were purchased from Corpuscular Inc. and Bangs Laboratories, respectively. 1-Ethyl-3-(3-dimethyl-aminopropyl) carbodiimide hydrochloride (EDC) was procured from Thermo Fisher Scientific, *N*-hydroxysulfosuccinimide (Sulfo-NHS) was from ProteoChem, and *N*-(5-amino-1-carboxypentyl) iminodiacetic acid (AB-NTA) was from Dojindo. Methoxy-poly-(ethylene glycol)-5000 amido-proprionyl methanethiosulfonate (MTS-PEG5K) was purchased from Toronto Research Chemicals, and carboxy-ethylsilane was from Gelest, Inc. Bio-Beads SM-2 was acquired from Bio-Rad Laboratories. All detergents were purchased from Affymetrix, and lipids were from Avanti Polar Lipids, Inc. All other chemicals were from Research Product International Corp., Thermo Fisher Scientific, or Sigma-Aldrich.

### Surface engineering of silica beads

10 mg of silica beads was washed twice with 1 ml Milli-Q $H_2O$ (EMD Millipore) before being equilibrated and resuspended in 1 ml of 0.10 M Na-phosphate buffer, pH 7.4. After the addition of 80 µl carboxy-ethylsilane, the bead suspension was rotated overnight at room temperature. The next day, the beads with carboxylates introduced by oxidization were washed three times with Milli-Q $H_2O$ and three times with 1 ml of 0.10 M MES buffer, pH 5. During the three washing steps, the beads were spun out of the aqueous phase at 8,000 rpm for 2 min in a tabletop centrifuge. After the wash, they were incubated with 2 mg/ml EDC and 2 mg/ml Sulfo-NHS in 0.10 M MES buffer, pH 5, for 1 h at room temperature. After the EDC/NHS conjugation, they were washed three times with 1 ml of 0.10 M bicine buffer, pH 7.5, and then incubated with 2 mg/ml AB-NTA in 0.10 M bicine buffer, pH 7.5, for 2 h at room temperature. The surface reaction on the beads was subsequently quenched with 0.10 M glycine (or galactosamine) for 1 h at room temperature. Finally, the NTA-conjugated beads were washed with $H_2O$, incubated with 0.10 M $Ni^{2+}$ for 30 min at room temperature, and equilibrated with a desired buffer for further experiments (Llaguno et al., 2014).

### Biochemical preparation of KvAP and its reconstitution into bSUMs

Recombinant KvAP was expressed and purified by following a published procedure (Jiang et al., 2004). A hexa-histidine tag added to the C terminus of the channel was used to bind the channel protein to the chemically functionalized beads (Fig. S1).

For membrane reconstitution, 0.10 mg of His-tagged proteins was bound to the Ni-NTA groups on the surfaces of the 10-mg beads. After the removal of unbound protein, the beads were washed with 5 mM decylmaltoside (DM) buffer so that only the channels bound to the surfaces of the beads had the opportunity to interact with lipids. Next, the protein-bound beads (10 mg) were incubated with 1 ml of 5 mg/ml of lipid mixture made of 1-palmitoyl-2-oleoyl-*sn*-3-glycero-phospho-ethanolamine (POPE)/1-palmitoyl-2-oleoyl-*sn*-3-glycero-phospho-glycerol (POPG) at a weight ratio of 3:1 (PE/PG hereafter) or other lipids (DOPC, POPC, etc.). The lipids were fully solubilized in 10 mM HEPES, pH 7.4, 200 mM KCl, and 40 mM DM. After incubation overnight at 4°C, the detergents in the mixture were slowly removed via Bio-Beads SM-2. The total weight of the Bio-Beads was 100 mg for the first hour, and these were replaced sequentially every hour with 70, 50, and 30 mg of freshly cleaned Bio-Beads, respectively. This step-wise changing of the Bio-Beads was found to be critical in supporting bilayer formation around individual beads, probably because fast removal of detergents made it easy to form smaller vesicles, instead of continuous bilayers around individual beads. Excess lipid vesicles were washed away after reconstitution. To confirm that the reconstitution was successful, the reconstituted channels were extracted and examined via SDS-PAGE (Fig. S1).

### Fluorescence microscopy of labeled bSUMs

KvAP channels on the surfaces of the beads (5 µm) were labeled with 0.10 mg/ml of variable fragment of the 33H1 antibody (Fv) that is labeled with Alexa Fluor 488 (Fv–Alexa Fluor 488) (Zheng et al., 2011) in a buffer containing 10 mM HEPES/KOH pH 7.4, 200 mM KCl, and 1 mg/ml BSA; washed with the same buffer; and visualized in a fluorescence microscope (Axioplan 2E; Carl Zeiss). The Fv used here contained a single immunoglobulin domain that was derived from a monoclonal antibody specifically targeting the S3–S4 loop of the voltage-sensor domain in the KvAP channel when the voltage-sensor domain is in the activated ("UP") conformation (Zheng et al., 2011). The highly specific Fv binding allows nearly absolute certainty in affirming the KvAP channels in bSUMs. To visualize the lipid bilayers on the surface of the bSUMs, the beads were incubated with 0.50 µg/ml FM1-43 (Invitrogen) for 5 min on ice. FM1-43 fluoresces strongly when inserted into a hydrophobic membrane. After three washes with the buffer, the beads were sandwiched between a glass slide and a coverslip and examined under a fluorescence microscope (Carl Zeiss). The fluorescent images were captured using a monochrome CCD camera (C-4742-95; Hamamatsu Photonics). Similarly, fluorescently labeled charybdotoxin (CTX) was used to visualize the channels in the bSUMs (not depicted).

### Cryo–electron microscopy (cryoEM) imaging of bSUMs

Because of the limited thickness of the vitrified ice in cryoEM specimens, we used silica beads of 0.20 µm in diameter to prepare KvAP-containing bSUMs using the same procedure described above. 4 µl of silica beads or bSUMs (0.10 mg/ml) in suspension were loaded onto glow-discharged copper grids that were coated with holey carbon films (Quantifoil grids; Structure Probe, Inc.). Inside a Mark III Vitrobot (FEI), the grids were blotted for 4 s, immediately plunged into liquid ethane, and stored in liquid nitrogen until EM examination. For cryoEM imaging, the grids were transferred into a transmission electron microscope (JEM 2200FS; JEOL USA, Inc.) operated at 200 kV. Pictures were taken with an electron dose of ∼20 electrons per $Å^2$ at defocus levels varying from −1.5 to −3.5 µm and digitized directly in a CCD camera (UltraScan 1000XP; Gatan, Inc.).

### Gel-shift assay of single-cysteine KvAP mutants

The bSUMs made of KvAP cysteine mutants (5 µm) were reduced with 5 mM DTT at room temperature for 30 min, gently spun down at 1,000 *g* for 5 min at 4°C, and washed twice with a DTT-free buffer (10 mM HEPES/KOH pH 7.4, 200 mM KCl) before being reacted with 0.50 mM MTS-PEG5K at room temperature for 30 min. The cysteine-specific reaction was stopped with 10 mM iodoacetamide. 20 mM DM and 300 mM imidazole were added to extract the KvAP protein before the protein was assayed via Coomassie blue–stained nonreducing SDS-PAGE.

### Electrical recordings of ion channel activity in bSUMs using planar electrodes

A Port-a-Patch system using planar glass chips (electrodes) was purchased from Nanion Technologies. A tabletop vibration isolation system (Warner Instruments) was used to support the recording system inside a Faraday cage. Disposable glass chips, which

usually have a serial resistance of 1–10 MΩ and were purchased from Nanion Technologies, were pretreated by adding 1 µl of 20 mg/ml of lipids in decane around the hole in a planar electrode. Under reflected light, the small hole in the electrode could be spotted. Care was taken to spread the lipids in decane at least 1 mm away from the tiny hole. The decane solution had the same lipid composition as the bSUMs, and after pretreatment, it was allowed to dry out completely. No bilayer was ever found to form across the hole in an electrode at this stage, which was confirmed by measuring the serial resistance of the electrode and by examining the holes under a microscope. To confirm that no materials obstructed the hole, we examined the glass electrodes under a phase-contrast microscope. The dried lipids on the glass could be recognized around the electrode hole. Even though it is not required for seal formation, the pretreatment was found to enhance the success rate of gigaohm seal.

After pretreatment, the glass chip was mounted into the Nanion Technologies recording system. The buffer in the top partition contained 80 mM NaCl, 200 mM KCl, 1 mM $MgCl_2$, 2 mM $CaCl_2$, and 10 mM HEPES/NaOH, pH 7.4, and that in the bottom partition contained 10 mM NaCl, 200 mM KCl, 60 mM KF, 20 mM EGTA, and 10 mM HEPES/NaOH, pH 7.4. In all cases, we used the same solutions unless otherwise specified. At the beginning of each experiment, the electric potential difference between the two electrodes was balanced under zero-current conditions. Because we used solutions containing high concentrations of NaCl, KCl, or KF, the liquid junction potentials between the solutions on the two sides of the electrode were expected to be only a couple of millivolts and were neglected (Table 1). Premade bSUMs in suspension (10 mg/ml; ∼30 µg was added each time) were pipetted into the top partition of the glass chip just above the hole, which could be seen from the reflected light. Sometimes, a 20× dissecting stereomicroscope was used to help locate the hole in a mounted glass chip. If a bead happened to land on the hole because of gravity, the seal resistance would go up. Because of the large number of beads (∼50,000) added into the top partition, which if densely packed next to one another, would cover an ∼3.5 × 3.5–$mm^2$ surface area on the glass chip, it was often fairly easy to have one bead fall squarely to the top of the hole. If no bead landed on the hole within a few minutes, we usually pipetted the solution in the top partition to agitate the beads or added more beads. If nothing happened after a few trials, we usually restarted the experiment with a fresh glass chip. A test pulse of 10 mV was used to monitor the seal resistance continuously during this process. As soon as the seal resistance went up by 5–10 MΩ, the solution in the top partition (20 µl in total; above the glass chip) was exchanged with small aliquots (5 µl) of the seal-enhancer solution (80 mM NaCl, 200 mM KCl, 10 mM $MgCl_2$, 35 mM $CaCl_2$, and 10 mM HEPES/NaOH, pH 7.4). After that, a gigaohm seal was usually formed within a few minutes. The buffer in the bottom partition, which is below the glass electrode and corresponds to the extravesicular side of the bSUMs or the extracellular side of KvAP channels anchored through their C-terminal His-tags, contained 10 mM NaCl, 200 mM KCl, 60 mM KF, 20 mM EGTA, and 10 mM HEPES/KOH, pH 7.4. After the stabilization of the sealed patch, the solution in the top partition was replaced with a buffer containing 80 mM NaCl, 200 mM KCl, 1 mM $MgCl_2$, 2 mM $CaCl_2$, and 10 mM HEPES/NaOH, pH 7.4. Every 1–2 min, a test pulse from a holding potential of −80 mV to a test potential of 80 mV for 200 ms was delivered to examine the channel activity. Electrical recordings from bSUMs in the inside-out mode (Fig. 1 E) were performed as described previously (Zheng et al., 2011). The currents were recorded with an amplifier (Axopatch 200B; Molecular Devices), filtered at 2 kHz, and sampled at 5 kHz. The analysis of the electrophysiological data was performed with both Clampfit (Molecular Devices) and IGOR Pro 6 (WaveMetrics).

## Online supplemental material

We followed the KvAP protein that went through the steps of making bSUMs in Fig. S1, and compared the clamping speeds on bSUMs with that from BLMs in Fig. S2. In Fig. S3, we presented more details on the analysis of tail currents, which followed the same procedure used to estimate reversal potential in Fig. 7 (C and D). The online supplemental material is available at http://www.jgp.org/cgi/content/full/jgp.201511448/DC1.

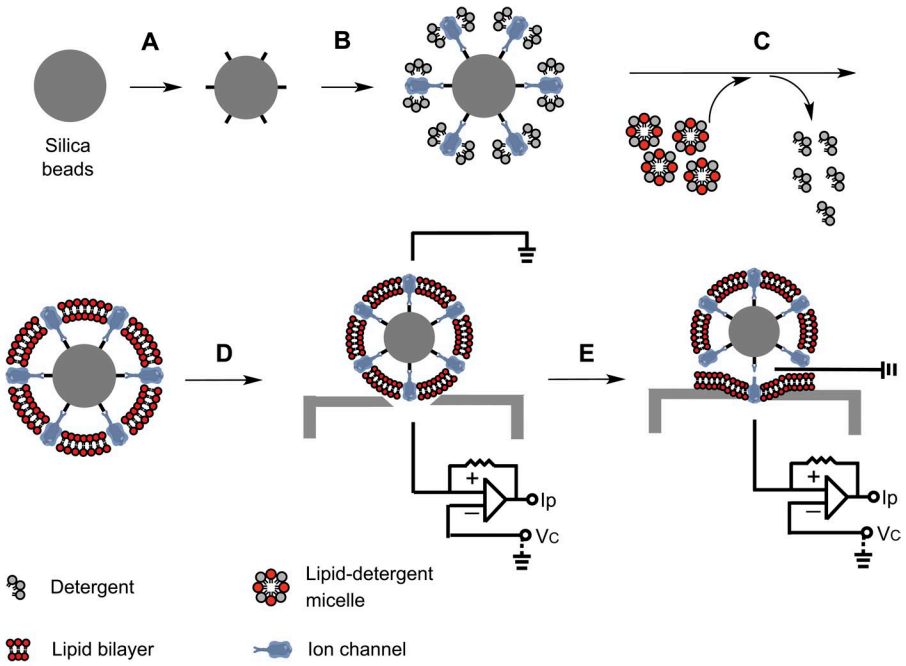


**Figure 1.** Chemical principles behind the formation of bSUMs. (A) Surface functionalization through chemical oxidization and bioconjugation. (B) Binding of transmembrane proteins via active ligands on the surface of the beads. (C) Reconstitution of a lipid bilayer around the anchored membrane proteins on the beads. (D) Electrical recordings from reconstituted channels in bSUMs by using a planar electrode, which would be equivalent to a cell-attached patch. (E) After the formation of gigaohm seal on a planar electrode, the vesicle of a bSUM usually ruptures outside the sealed area and leads to the opening from the top partition to the intravesicular side of the bSUM, similar to an excised patch (inside-out mode).

## RESULTS

### Scheme for reconstituting bSUMs

The main idea is to construct a bilayer system that allows us to introduce various types of lipids often seen in eukaryotic membranes while at the same time enabling the proper reconstitution of target membrane proteins. As depicted in Fig. 1, the key requirements for the bSUM system include a high density of functional groups on the surface of a bead, which allows for the efficient and selective binding of transmembrane proteins in detergents and the proper reconstitution of a bilayer. After the lipid/detergent solution is introduced, Bio-Beads are added to remove the detergents. The slow removal of detergents allows enough time for lipids to fill the space between the surface-anchored membrane proteins, which are, on average, 30–50-nm apart (Fig. 1 C). The hydrophobic packing between lipid molecules around individual membrane proteins drives the reconstitution of a continuous lipid membrane. Because the membrane proteins act as membrane-organizing centers, their orientation is primarily determined by their radial attachment to the spherical beads. The hydrophobic interactions between proteins and lipids will promote the formation of a single lipid bilayer (unilamellar membrane). After the membranes form, the beads can be loaded onto a planar electrode and form a gigaohm seal for electrical recording (Fig. 1 D). Our further experiments also found (see the experiments showed in Fig. 6 B) that in practice, the membrane above the sealed area usually ruptured, and the intracellular side of the patch became exposed to the top partition, which is equivalent to the configuration of an excised inside-out patch (Fig. 1 E).

### Chemical engineering of the beads and the insertion of KvAP channels into bSUMs

We first tested the feasibility of chemical engineering on the surface of silica beads. Under a scanning electron microscope, the silica beads used in our experiments showed fairly smooth surfaces and appeared almost perfectly spherical (Fig. 2 A). It was thus reasonable to use them to support the formation of large-dimensional unilamellar membranes. After the introduction of surface carboxylate groups via oxidization, we used the EDC/NHS reaction to convert the carboxyl groups into Sulfo-NHS esters (Fig. 2 B). The good leaving groups in the Sulfo-NHS esters make them very reactive to primary amine groups. The reactive beads were then incubated with AB-NTA. The primary amine of the latter was used to link the NTA to the bead surface. The NTA groups on the beads were subsequently charged with $Ni^{2+}$ (Fig. 2 B). Recombinant green fluorescent protein (GFP) with a C-terminal His-tag (GFP-$His_6$) was prepared to biochemical purity and used to quantify the selective binding of the His-tags to the

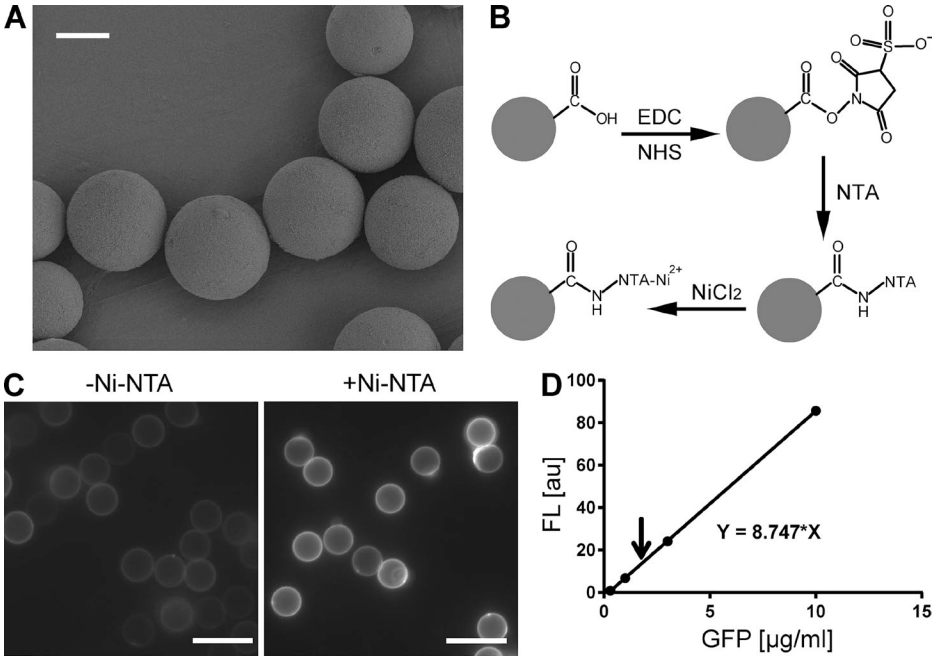


**Figure 2.** Functionalization of silica beads with Ni-NTA groups. (A) Scanning electron microscopic (SEM) images of 10-µm micrometer beads. Bar, 5 µm. (B) Diagram of chemical functionalization on the surface of an oxidized silica bead. Only one carboxylate is drawn for simplicity. EDC/NHS was used to accelerate conjugation reaction and maximize reaction efficiency. (C) Fluorescent images of functionalized beads labeled with GFP-$His_6$ proteins. Beads that were functionalized in the absence (left) or presence (right) of AB-NTA were compared. The latter showed significant labeling (right), suggesting a high density of Ni-NTA groups on the surface. Bars, 10 µm. (D) Estimation of the binding capacity of the surface Ni-NTA groups. A standard curve of fluorescence intensity was first prepared (dots and the continuous line). 0.10 mg GFP-$His_6$ was incubated for 2 h with 10 mg Ni-NTA silica beads in 0.40 ml buffer containing 10 mM HEPES/KOH, pH 7.4, and 200 mM KCl. After the removal of unbound GFP-$His_6$, the bound GFP-$His_6$ was eluted with 0.30 M imidazole, and its fluorescence intensity (the arrow) was measured and compared with the standard curve. The measured signal corresponded to ~0.84 µg GFP-$His_6$ for 10-mg beads, which is ~19 trillion GFP molecules. Based on the manufacturer's information, the total surface area of the 10-mg beads is $5.8 \times 10^9$ $\mu m^2$. The estimated binding capacity of the Ni-NTA beads is ~3,300/$\mu m^2$.

Ni-NTA groups on the bead surface (Fig. 2 C, right). Without Ni-NTA treatment, the binding of GFP-$His_6$ on the beads was difficult to detect (Fig. 2 C, left). To quantify the amount of bound GFP-$His_6$, a standard fluorescence intensity curve as a function of GFP-$His_6$ concentration was first prepared in the same buffer (Fig. 2 D, dots and the continuous line). 0.10 mg GFP-$His_6$ was incubated with 10 mg of Ni-NTA–presenting silica beads in 0.40 ml buffer containing 10 mM HEPES/KOH, pH 7.4, and 200 mM KCl. After the incubation and removal of unbound GFP-$His_6$, the bound GFP-$His_6$ on the beads was eluted with 0.40 ml buffer containing 300 mM imidazole, and its fluorescence was measured (Fig. 2 D, arrow) and compared with the standard curve. The concentration of the eluted GFP-$His_6$ was estimated by comparing its fluorescence intensity with a predetermined standard curve. The total surface area of the 10-mg beads was used to make a reasonable estimate of the surface-binding capacity of the beads, $\sim$3,300/$\mu m^2$.

Next, we assessed whether it was possible to introduce membrane proteins and lipid molecules to the functionalized beads and then slowly remove the detergents to drive the formation of lipid membranes on the surfaces of the beads. Because of its high stability in various detergents and lipids, KvAP, a Kv channel originally identified from a thermophilic archaebacterium, *Aeropyrum pernix* (Ruta et al., 2003), was introduced as a model system. Recombinant KvAP-$His_6$ was expressed in bacteria and purified to biochemical homogeneity. To ensure the interaction between Ni-NTA and the hexa-histidine tags, 0.10 mM PMSF was always present in all reconstitution steps to minimize the potential proteolytic loss of His-tags from the C terminus of the recombinant protein. After mixing the protein-bound beads with PE/PG (3:1) in the detergents, the stepwise removal of the detergents using Bio-Beads was executed to reconstitute the bilayer membranes around the surface-anchored channels.

Because the formation of continuous bilayers was critical to our intended electrical recordings of reconstituted channels, we developed two assays with which to examine the integrity of the bilayers and the proper reconstitution of the channel proteins in them. In the prepared bSUMs, we demonstrated the presence of a membrane by using FM1-43, a fluorescent dye, which becomes brightly fluorescent when inserted into a hydrophobic environment (Fig. 3 A). Because the surfaces of our functionalized beads were hydrophilic, it was very unlikely that a monolayer would form and allow FM1-43 to fluoresce. The DIC images showed the location of individual beads, and the FM1-43 fluorescence images highlighted a continuous layer of membranes around every bead that was preincubated with the KvAP protein (Fig. 3 A, bottom row). Because the fluorescence emission of FM1-43 is much stronger in a hydrophobic environment, such as a lipid bilayer in which the lipophilic tail of an FM1-43 is inserted into one leaflet of the membrane, than in a polar solvent (Gaffield et al., 2006), the fluorescence images in Fig. 3 A suggested the presence of seemingly continuous lipid membranes on the surfaces of individual beads. On some bSUMs, there were tiny fluorescent puncta (Fig. 3 A, red arrow in the bottom right), which likely resulted from small vesicles ($\sim$200 nm in diameter) attached to the bead-supported membranes. We found that washing the beads with a buffer containing a slightly lower concentration of salts ($\sim$100 mM KCl) could help release most of these attached vesicles into the bulk solution

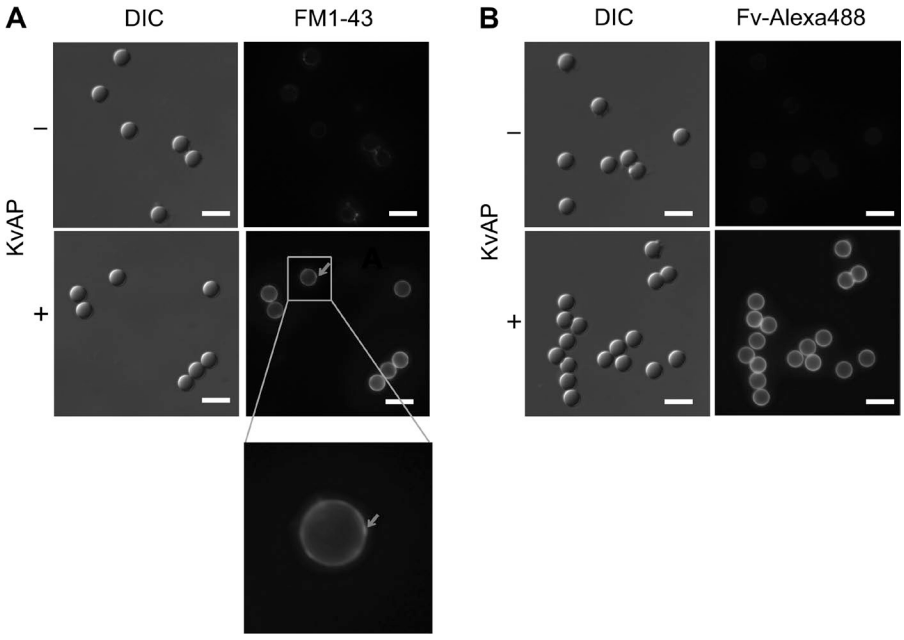


**Figure 3.** Surface-anchored ion channels guide the formation of bSUMs. KvAP channels were used as a model system to form bSUMs around silica beads. The bSUMs around the beads of 5 μm in diameter were stained with FM1-43 (A) or with the KvAP-specific Fv–Alexa Fluor 488 (B). The fluorescence images (right) were shown side-by-side with the DIC images (left). Without KvAP, no fluorescence was seen around the beads (top rows). There was weak, nonspecific binding of FM1-43 to the beads. With KvAP, in bSUMs, there was uniform, circular staining around individual beads by FM1-43 and Fv–Alexa Fluor 488 (bottom right in both A and B). The integration of the epifluorescence signal made the edge of a vesicle much brighter than its center. The red arrow in A points to a small puncta, which is better seen in the zoomed-in view underneath and is quite likely caused by the attachment of a small vesicle. Bars, 10 μm.

phase so that they would not interfere with the seal formation on glass electrodes.

To test whether the KvAP channels in the bSUMs were reconstituted in the expected orientation from their surface anchorage through the intracellular His-tags, we used fluorescently conjugated Fv–Alexa Fluor 488 to label them from the outside of the bSUMs. This experiment does not exclude the possible incorporation of a small fraction of channels in the opposite orientation (see next section). As described previously (Zheng et al., 2011), the Fv fragment recognizes the loop between the third (S3) and fourth (S4) transmembrane segments of the KvAP voltage-sensor domain when the latter is in the activated (UP) state at 0 mV. Alexa Fluor 488 was covalently linked to the Fv fragment on a site (A61C of the heavy chain) that is diagonal from its epitope-binding site and thus does not interfere with epitope–Fv interaction. When the beads had no protein, the binding of Fv–Alexa Fluor 488 was nearly undetectable (Fig. 3 B, top row). In contrast, on the beads that were preincubated with the KvAP proteins, the Fv–Alexa Fluor 488 binding gave rise to strong signals (Fig. 3 B, bottom row). Every bead had an even fluorescent ring around it. The relatively uniform fluorescence signal around many beads suggested an even distribution of the KvAP channel protein on their surfaces, which was expected because of the randomly Poisson-distributed binding sites on the Ni-NTA beads. Also, the projection along the optical axis made the epifluorescence signal at the edge of a bSUM stronger than that in the middle of the images, giving rise to the hollow darkness in the center, similar to the epifluorescence images of individual giant unilamellar vesicles (GUVs; see Fig. 8 in Aimon et al., 2011).

These two lines of evidence support the idea that the KvAP channels on the surface of the beads drove the formation of lipid membranes. As expected, the guided binding of the intracellular sides of the channels to the beads caused a major fraction of channels to have their extracellular side facing the outside of the bSUMs. The membranes around individual beads were apparently even and continuous and appeared suitable for patch-clamp recordings.

### The unilamellar nature of the bSUMs

Our labeling of the membranes and the proteins with FM1-43 and Fv–Alexa Fluor 488, respectively, was sufficient to demonstrate the presence of seemingly continuous lipid membranes. Because of the limited resolution of fluorescence microscopy, we could not distinguish a continuous membrane from a collection of discontinuous patches of lipid membranes or tiny unilamellar vesicles at the nanometer scale; nor were we able to separate one bilayer from a stack of multiple bilayers. To further characterize the shape and structural features of the bSUMs, we examined these supported membranes via cryoEM. Because of the limited penetration of the electron beam in ice (<500 nm), we applied the same surface chemistry and reconstitution procedures to form bSUMs around silica beads that were 200 nm in

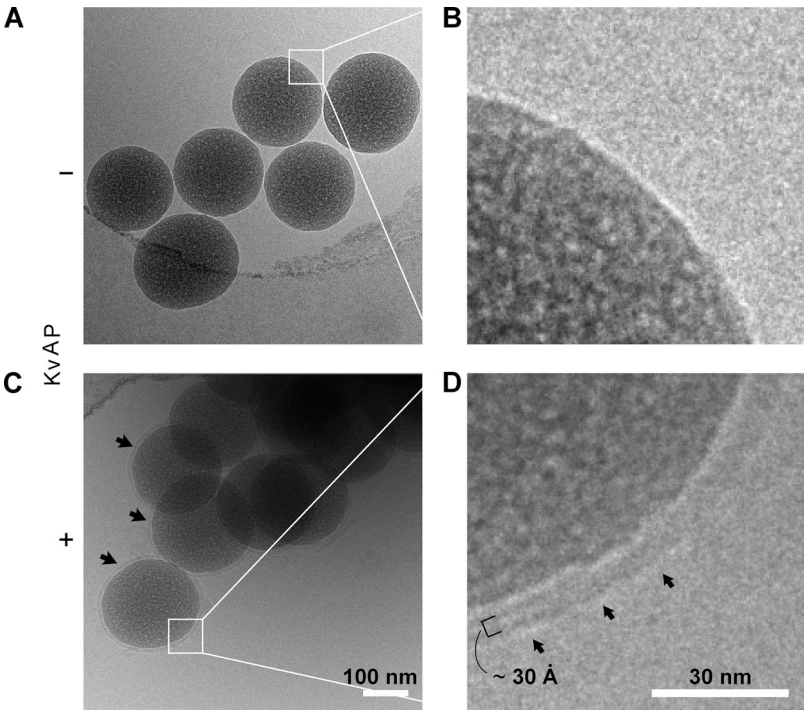


**Figure 4.** Unilamellar nature of bSUMs revealed by cryoEM. Beads of 0.20 µm in diameter were used to prepare the specimens. A PE/PG lipid mixture was used for membrane reconstitution. Beads prepared in the absence (A and B) or presence (C and D) of KvAP protein were compared under cryoEM. Multiple beads trapped close to the edge of a hole in a holey carbon–coated Quantifoil grid are shown in each image (A vs. C). The black arrows in C point to membranes around individual beads. B and D represent magnified views of the two areas marked with white squares in A and C, respectively. There is no clear membrane at the bead surface in B, but a characteristic bilayer structure (after convolution of the contrast transfer function of the EM) is seen in D. In D, the arrows mark the outer surface of the bSUM. The small black bracket, covering two dense bands and one light band, represents the thickness of the hydrophobic core of a typical bilayer, ~3 nm.

diameter. These bSUMs were loaded onto Quantifoil holey grids and plunge-frozen in the same buffer solution in which they were prepared. The samples were observed with nominal defocus levels of −2 to −3 μm. Even though the surface curvature in these small bSUMs is higher than those around the beads with larger diameters, the fundamental lipid arrangement character on the smaller beads should closely reflect that of the bSUMs on the surfaces of larger ones because the surface density of the anchored proteins and the reactive groups were the same, and the reconstitution process was dictated by the densely anchored membrane proteins.

Indeed, the cryoEM images showed a single bilayer (unilamellar) structure on the surface of each of those beads that were preincubated with the KvAP proteins (Fig. 4, C vs. A). Every bead had one and only one bilayer (Fig. 4 C, arrows) covering its surface continuously. We were able to follow the bilayer structure on every bead in Fig. 4 C, meaning that the bilayer was smooth and continuous. Enlarged images of the membranes on the beads showed two-electron–dense bands, with one light band between them (Fig. 4 D with Fig. 4 B as control), a typical bilayer structure after the convolution of the EM contrast transfer function, the same as previously seen in the cryoEM images of lipid vesicles (Jiang et al., 2001). The thickness of the hydrophobic core in the bilayer was estimated by measuring the distance from one dark band to the other in the projection image and was found to be ∼3 nm (Fig. 4 D), which is close to the average thickness of the hydrophobic core in a typical phospholipid bilayer containing 16–18 carbon acyl chains in each leaflet (Lewis and Engelman, 1983). These cryoEM images led us to the fairly firm conclusion that anchored transmembrane proteins (KvAP in our case) are able to reconstitute a single continuous bilayer membrane around each bead. Although the 120-kD KvAP tetramers were still too small to be recognized under cryoEM, these images clearly showed that our new bSUM system is unilamellar.

### Favored directional insertion of tetrameric channel proteins in bSUMs

Before constructing a suitable system with which to record voltage-dependent activity from the ion channels in bSUMs, we further examined the biochemical integrity of the channel proteins in the bSUMs. We first confirmed that the KvAP channels in the bSUMs could be extracted with detergents and imidazole, via size-exclusion chromatography run in the same place as the KvAP channels purified from bacteria (Fig. 5 A, red trace), and were detected as a single band in SDS-PAGE (Fig. 5 B). The peak width in the gel-filtration profile for the detergent-extracted channels from bSUMs was slightly broader than the KvAP directly purified from *Escherichia coli*, probably because of the lipids that resulted from the detergent extraction. These data suggested that the channel proteins in the bSUMs remained folded and properly assembled as tetramers.

Previously, Fv binding was used to detect the channels from the extravesicular side to confirm that the channels were oriented as we expected. However, an Fv-binding assay does not guarantee 100% unidirectional orientation. To further test our prediction, we measured the accessibility of single cysteine mutants, L125C, in bSUMs. To examine cysteine accessibility, we used MTS-PEG5000 (MTS-PEG5K) to react with the sulfohydryl (−SH) groups within a 30-min period. When the cysteine is conjugated, the modified protein will be ∼5 kD heavier than the control protein in SDS-PAGE

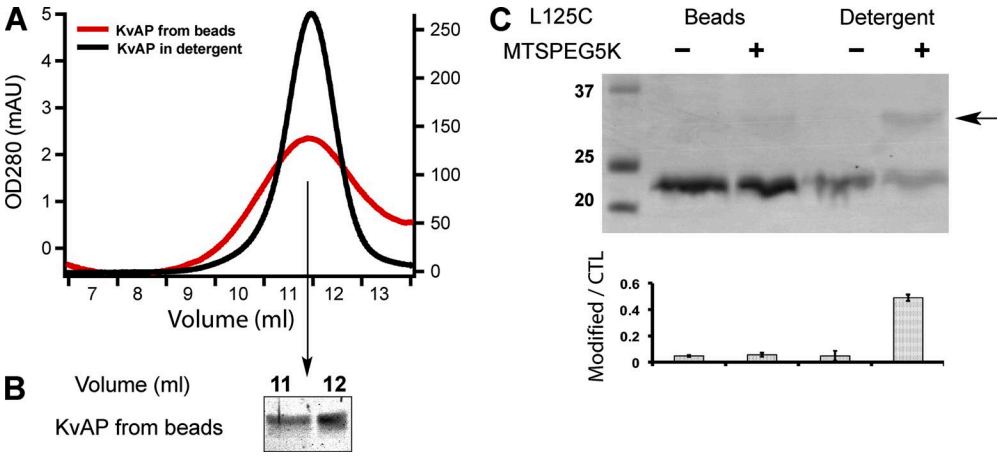


**Figure 5.** Unidirectional insertion of tetrameric Kv channels in bSUMs. (A) KvAP from bSUMs remains tetrameric. KvAP was extracted from the bSUMs by 40 mM DM, concentrated, and injected into a Superdex 200 size-exclusion column. The channels were eluted (red line) at the same position as those purified in detergents (black line). The slightly broader peak width could be caused by the lipids. (B) KvAP from the elution peak in A was collected and assayed via Coomassie blue–stained reducing SDS-PAGE. The channel protein showed no detectable degradation. (C) Inaccessibility of KvAP L125C in the bSUMs made of PE/PG lipids. KvAP in bSUMs or extracted in 40 mM DM were treated with MTS-PEG5K before being assayed by Coomassie blue–stained nonreducing SDS-PAGE. PEG5K conjugation shifted the channel band by ∼5 kD (arrow to the right side). The density ratio of the conjugated protein versus the unconjugated control (CTL) was plotted underneath the gel (bottom). The errors bars showed the range of variation from duplicate measurements. This experiment was repeated more than four times by different authors.

(Fig. 5 C, black arrow; Zheng et al., 2011). As a positive control, we showed that the L125C KvAP in bSUMs treated with detergents was reactive, probably because of the mobility of the voltage-sensor domains in the detergents (Fig. 5 C, rightmost lane), which also suggested that the L125C −SH groups remained reactive after their reconstitution into bSUMs. Comparison of the integrated intensities for individual bands in the SDS-PAGE gel (Fig. 5 C, bar graph) confirmed that ∼32% of the total L125C protein was modified in detergents within a short period of reaction time, but there was no significant modification of the L125C channels in the bSUMs.

Our previous studies showed that when the KvAP voltage-sensing domains are in the UP conformation (Zheng et al., 2011), the L125C in the S4 helix (just above the fourth arginine residue) is fully embedded in the membrane and therefore inaccessible from either side of a phospholipid membrane, which is similar to what was reported previously in the *Shaker* K channel (Yang et al., 2004). When the VSDs are in the DOWN conformation, L125C becomes accessible to the intracellular side. As expected, L125C KvAP in bSUMs made of PE/PG was completely inaccessible to MTS-PEG5K in different conditions (Fig. 5 C, the second lane), suggesting that L125C faced the intravesicular sides of the bSUMs and was shielded by the membrane from being chemically modified by the membrane-impermeable MTS reagents. To vary the bSUM transmembrane potential, we performed the reactions in various potassium concentrations outside (10, 150, and 1,000 mM) and were not able to conjugate the cysteine residues to a significant level. 1 M KCl outside would make the bSUM membrane depolarized (inside positive, ∼60 mV). Under such conditions, the channels with their intracellular side facing outside (the opposite of what we

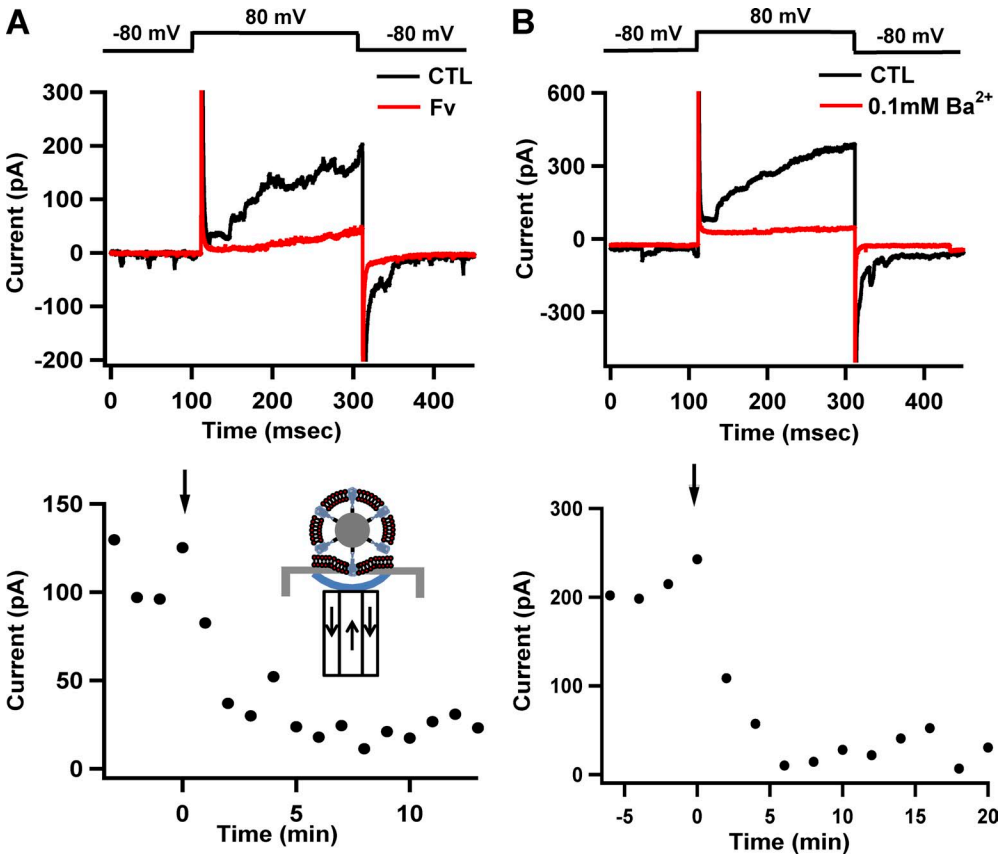


**Figure 6.** Electric recordings of tetrameric Kv channels in bSUMs. (A) Specific inhibition of the channel activity by Fv. After the formation of the gigaohm seal, test pulses from a holding potential of −80 to 80 mV for 200 ms were delivered once every minute. The gigaohm seal was formed in the cell-attached mode. As a result of membrane disruption on the outside (see B and Fig. 1 E), recordings were made in the inside-out mode (black trace in the top panel). When 100 µg/ml Fv was perfused into the extracellular side of the channels for 2 min while the membrane was held at 0 mV (inset diagram to the bottom), the channel activity was almost completely blocked (red trace). The bottom panel displays the time-dependent inhibition of KvAP activity via Fv. The black arrow points to the time of Fv application. The arrows in the cartoon of the bottom show the solution flow (arrows) to and from the bottom droplet (blue line) right under the hole of the planar electrode in the perfusion system. The results represent typical experiments from many of our routine tests to confirm the identity of the recorded channels. (B) Breakdown of the bSUMs on the outer side (above the planar electrode) after the formation of the gigaohm seal avoids the space-clamp problem. After the recorded currents became stable (black trace in the top panel) for at least 10 min, 0.10 mM $Ba^{2+}$ was perfused into the top partition, and the currents were recorded 2 min later. The top panel shows two traces before and after $Ba^{2+}$ addition (black and red traces, respectively). The bottom panel displays the time-dependent inhibition of KvAP activities by $Ba^{2+}$. The black arrow indicates the time when $Ba^{2+}$ was applied. These results are typical of four experiments. For these experiments, the solution in the top partition (the intravesicular side of the bSUMs and the intracellular side of the channels) contained 80 mM NaCl, 200 mM KCl, 1 mM $MgCl_2$, 2 mM $CaCl_2$, and 10 mM HEPES/KOH, pH 7.4; the bottom partition (the extravesicular side of the bSUMs and the extracellular side of the channels) had 10 mM NaCl, 200 mM KCl, 60 mM KF, 20 mM EGTA, and 10 mM HEPES/KOH, pH 7.4.

expected) would be hyperpolarized, and their L125Cs would become accessible from the outside. However, we did not see reliable reactions. On the other hand, should the membrane have any ruptures, MTS-PEG5K would be able to diffuse through and gain access to the intracellular side. We reasoned that if the KvAP were not properly folded or incorporated in the opposite orientation in the bSUMs, the L125C would become accessible and be detected through a chemical reaction. Our lack of reactivity with the L125C therefore suggests that a majority of the channels were oriented outside-out.

Our Fv-binding assay demonstrated that the reconstituted proteins were accessible from the outside and were not enclosed inside the bSUMs to avoid reaction with MTS reagents. We also confirmed that the channels were able to bind fluorescently labeled pore-blocking toxin (CTX), suggesting that the extracellular side of the pore domains faced the outside of the bSUMs (not depicted). All these results, together with the cysteine-accessibility tests in S4 and the fact that in the KvAP bSUMs the channels were anchored to the beads through the C-terminal (intracellular) His-tags, make a compelling argument that the majority, if not all, of the KvAP channels in the bSUMs were folded correctly and embedded in the supported bilayers, with their extracellular sides facing the outside of the vesicles in the bSUMs, and were thus suitable for electrical recording. Here, we use the term "unidirectional insertion" to reflect the observations supporting the idea that the majority of channels take the expected orientation but not in the absolute sense that would exclude the possibility of a small fraction of channels being either misfolded or mis-oriented. All our observations agree with such a notion. In order for us to say that there are absolutely no channels facing the opposite orientation, we would need a very fine counting of the channels with both orientations, as well as the misfolded ones, which is still experimentally challenging and not the main focus of our study. Our cryoEM is still not able to recognize the orientation of the channels. New assays will need to be developed.

### Electrical recordings from KvAP channels in bSUMs

Because of the direct linkage of the channels to the surfaces of the beads, the supported membranes are expected to be fairly stable and resistant to shearing force and deformation. The lack of flexibility in the membranes, however, could make it difficult to form a gigaohm seal with conventional fire-polished glass electrodes. We experimented with various shapes for the glass electrodes and various types of glass pipettes, without significant success in direct patch-clamp recording. As an alternative measure, we tested the formation of gigaohm seals by dropping the beads onto planar glass electrodes (chips) mounted in a Nanion Technologies Port-A-Patch system. Even though not absolutely required, the pretreatment of the planar electrode surface with lipids in decane was found to enhance the efficiency of gigaohm seal formation. Because of the complete drying of decane before seal formation with the bSUMs, we expect that no decane will enter the patched membranes. We found that the bSUMs could readily form tight seals with the planar electrodes (see details in Materials and methods), and electrical recordings from small patches (<1 µm) could achieve better temporal resolution than those from typical planar lipid bilayers (Fig. S2), whose high capacitance components were difficult to compensate for. When a patch was depolarized to 80 mV from a holding potential of −80 mV, the KvAP channels opened and conducted $K^+$ ions in a voltage-dependent fashion (Fig. 6, A and B, the control traces). Consistent with the observation that a majority of channels were favorably inserted in the outside-out orientation, no current was recorded when we switched the polarity of the test pulses (not depicted).

To confirm that the ion-conducting activity was indeed from the KvAP channels in the patched membranes, we took advantage of high affinity Fv fragments that were derived from a monoclonal antibody (33H1), recognized and immobilized the voltage-sensor domains of KvAP in their UP conformation, and thereby blocked the channel activity through steady-state inactivation. When Fv was perfused to the extracellular side of the channels in the membrane patches held at 0 mV for 2 min, the voltage-dependent activity of the channels was almost completely inhibited (Fig. 6 A, red trace in the top). The cartoon in the bottom panel in Fig. 6 A depicts the perfusion of the inner partition of the Nanion Technologies system, which corresponds to the extracellular side. The time-dependent Fv block showed that the action of the Fv protein on the channels happened within a few minutes (Fig. 6 A, bottom diagram, with an arrow pointing to the starting point of perfusion to the bottom partition of the Nanion Technologies system). The Fv binding was found to be irreversible within the short period of time the experiment lasted. The Fv effect also confirmed to the highest level of certainty that the channel activity was caused by the KvAP channels and not other unknown contaminants. Seals usually lasted for >30 min.

Considering the limited volume between the supported bilayer and the bead surface (Fig. 4 D), we expected to observe electric currents that were <200 pA and the exhaustion of current-conducting $K^+$ ions inside the bSUMs after the delivery of a few test pulses, which would pose a serious space-clamp problem. However, to our surprise and satisfaction, we were able to record multiple traces from the same patch repeatedly. The cryoEM images in Fig. 4 B also showed that the space underneath the membrane is rather limited. These observations suggested that the bilayer membranes outside the patch electrodes were probably broken, allowing the ions to

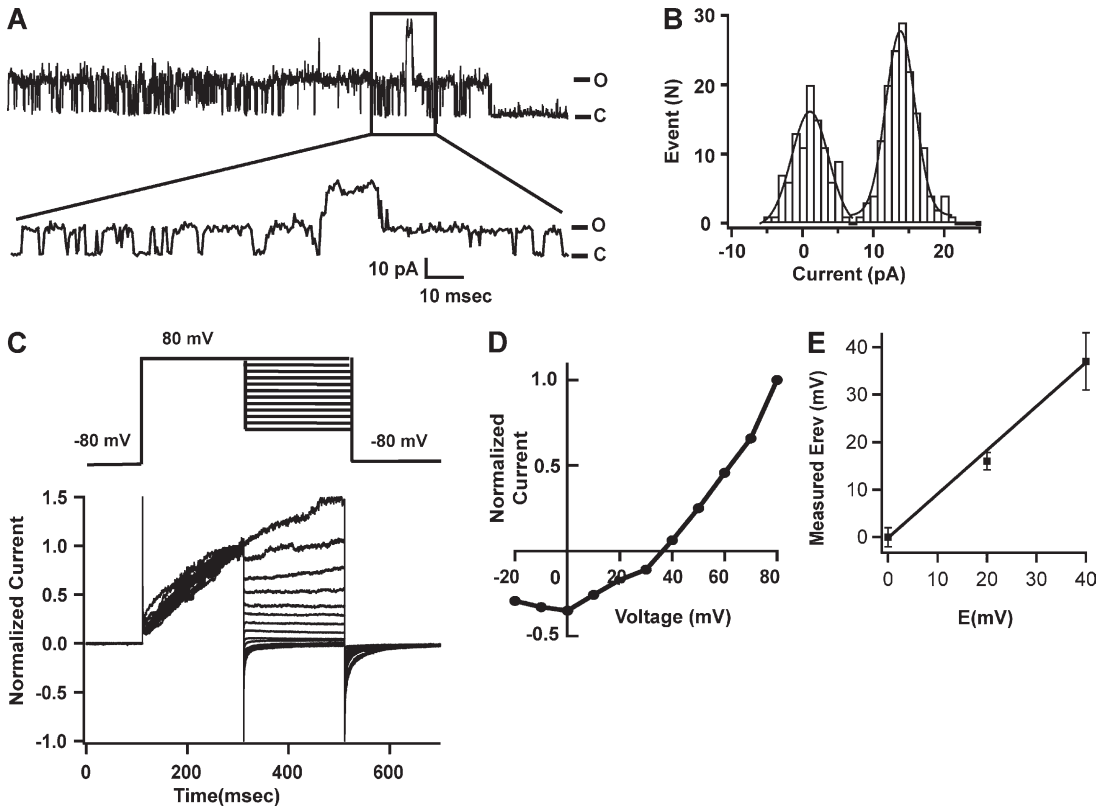


**Figure 7.** Electrophysiological properties of KvAP channels in bSUMs. (A) Single-channel activity at 80 mV. The windowed part was expanded and shown underneath. C, closed state; O, open state. There were at least two channels. The rareness of double openings suggested that the open probability at 80 mV was <50%. (B) Histogram of single-channel events at 80 mV. The peak value of the first channel opening is 14.3 ± 0.1 pA, and the baseline peak is 1.6 ± 0.3 pA based on Gaussian fitting. The calculated single-channel conductance is 174 ± 5 pS. (C) A typical series of current traces recorded from bSUMs using the pulse protocol is shown on the top. The bSUMs were prepared with solutions that set the Nernst potential for $K^+$ ions ($E_k$) to 0 mV. After depolarization to 80 mV for 200 ms, tail currents were measured at various potentials (−20 to 80 mV). For every trace, the leak conductance estimated at −80 mV was applied to all segments for leak subtraction. Only traces with very small or no leaks were used for analysis. The averaged tail currents during the first 20 ms of repolarization at various potentials were normalized against that at 80 mV and then used to make an I-V plot. A linear fitting around $I = 0$ was used to estimate the reversal potential. (D) A normalized I-V plot for $E_k$ = 40 mV is shown as an example. The reversal potential was found to be ∼38 mV. (E) Measured reversal potentials against $E_k$ in various potassium solutions. Each data point represents the average of two to four experiments, and the error bars represent the range of variation ($n$ = 2 for 20 mV) and the standard deviations ($n$ > 2 for 0 and 40 mV). The line represents a fitting with $y = a\,x$, yielding $a$ = 1.07 ± 0.1. The solutions used in these panels are listed in Table 1, with liquid junction potentials measured three times for each pair of solutions in a planar lipid bilayer setup.

diffuse into the space between the bSUM bilayer and the bead surface. Because the silica beads used in the bSUMs were solid and rigid, we suspected that the formation of the gigaohm seal over the hole of a planar glass chip might introduce local deformations around the rim of the hole and thus damage the bilayer structure next to the sealed patch. To assess this possibility, we added 0.10 mM $BaCl_2$ to the top partition of the planar electrode and found that $Ba^{2+}$ almost completely blocked the channel activity in the patched membranes within a few

TABLE 1

*Liquid junction potential measurements for solutions used in Fig. 7*

| Panels in Fig. 7 | $E_k$ | Intracellular | Extracellular | L.J. potential |
|---|---|---|---|---|
| | *mV* | *mM* | *mM* | *mV* |
| A and B | 6.6 | 80 NaCl, 200 KCl | 10 NaCl, 200 KCl, 60 KF | 0.40 ± 0.2 |
| C–E | 40 | 120 NaCl, 30 KCl | 90 KCl, 60 KF | 3 ± 0.4 |
| E | 20 | 80 NaCl, 70 KCl | 90 KCl, 60 KF | 2.6 ± 0.1 |
| C and E | 0 | 150 KCl | 90 KCl, 60 KF | 0.60 ± 1.1 |

The solutions used in Fig. 7 are listed above, with liquid junction (L.J.) potentials being measured three times for each pair of solutions in a planar lipid bilayer setup. Errors represent standard deviations calculated from three different measurements.

minutes (Fig. 6 B). Because of the tight gigaohm seal around the electrodes, we did not expect $Ba^{2+}$ to leak through the patch. The block must have occurred when the barium ions went through the membrane disruption, which probably resulted from the interaction of the lipid bilayer and the flat glass surface, and bound to the channels through the intracellular binding sites. Consistently, the IC50 of $Ba^{2+}$ from the intracellular side was previously reported to be <0.1 mM (Piasta et al., 2011), suggesting that our observed effect was caused by $Ba^{2+}$ binding to the channel pores from the intracellular side. These results support the idea that there were membrane ruptures or breakdowns on the top of the planar electrode, which allowed $Ba^{2+}$ ions to enter the limited space (slower diffusion than in bulk phase) between the bead surface and the bead-supported membrane and block channels from the intracellular side in the sealed patches. This also makes sense when we consider that the dried lipids added in a circular fashion around the holes in the electrodes helped stabilize the seal, probably because the broken membranes above the sealed patches flapped down and became attached to the lipids deposited on the glass electrodes (Fig. 1 E). An EM image of the sectioned electrode and bead will be needed to reveal such a structural change. We attempted to cut sections across fixed bSUMs but did not succeed in preserving the membrane integrity of the bSUMs. New methods are needed for preserving the patches for such an experiment.

Next, we measured some characteristic properties of the KvAP channels to determine whether the channel property remained similar in bSUMs, even though the channel kinetics, both activation and inactivation, seems to be different from those seen in bilayer recordings, which was also showed previously by Aimon et al. (2011). Using a planar electrode with a smaller hole (higher resistance, ∼5 MΩ or more), we were able to record single-channel activity at various holding potentials (at 80 mV, as an example; Fig. 7 A). From the histogram of single-channel events, the estimated single-channel conductance was ∼170 pS, close to what was first reported by Ruta et al. (2003) (Fig. 7 B). The high potassium concentration, from 150 to 250 mM, probably saturated the binding site inside the channel pore so that the single-channel conductance was not larger in our recordings.

To examine the ion selectivity of the recorded channels in bSUMs, we used tail currents at various voltages (Figs. 7 C and S3, A and B) to measure the reversal

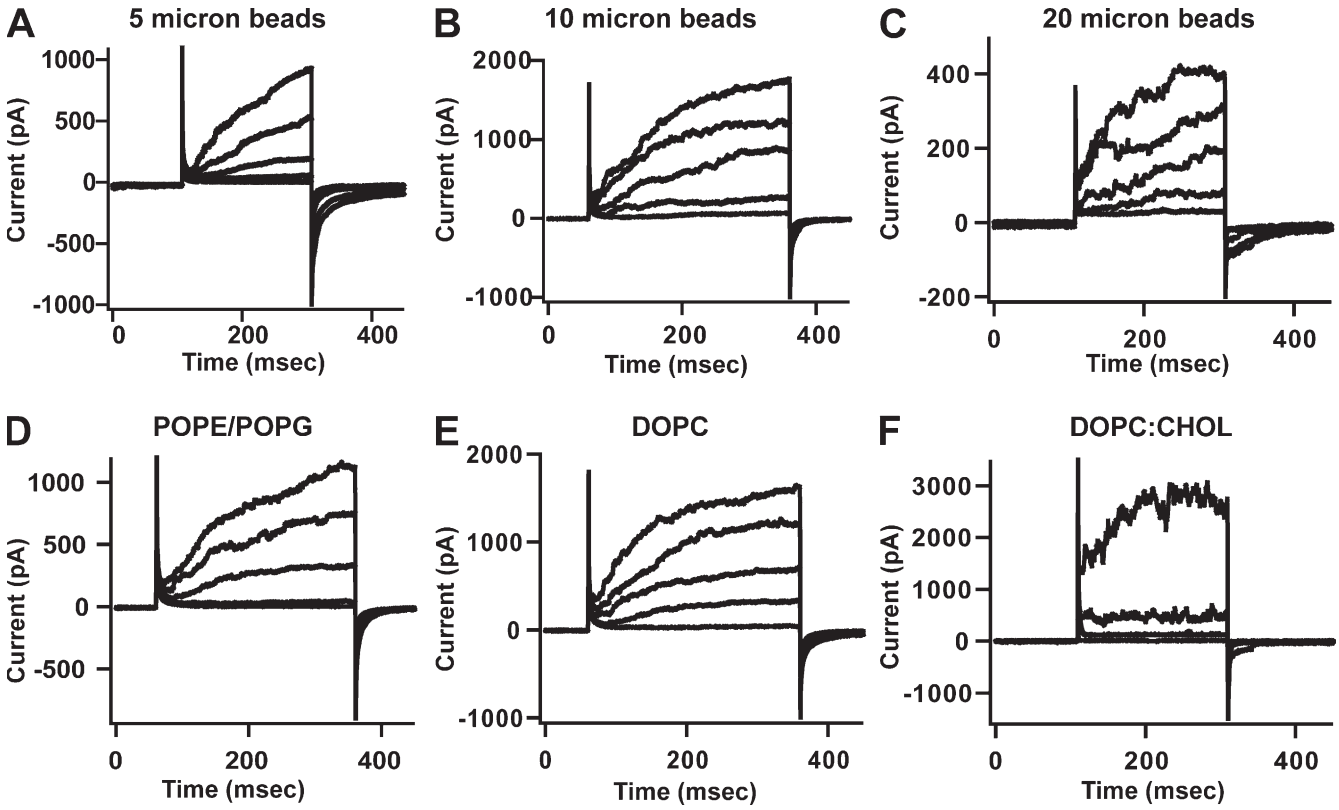


**Figure 8.** bSUMs of varying dimension and lipid composition. Electrical recordings from KvAP bSUMs of 5 (A), 10 (B) and 20 µm (C) in diameter, or made of different lipid mixture, 3:1 (wt/wt) POPE/POPG (D), DOPC (E), 95:5 (wt/wt) DOPC/cholesterol (F). Test pulses depolarizing from 0 to 160 mV at 40-mV steps were introduced every 2 min. The holding potential was −80 mV. The standard intracellular solution (80 mM NaCl, 200 mM KCl, 1 mM $MgCl_2$, 2 mM $CaCl_2$, and 10 mM HEPES/KOH, pH 7.4) and extracellular solution (10 mM NaCl, 200 mM KCl, 60 mM KF, 20 mM EGTA, and 10 mM HEPES/KOH, pH 7.4) were used.

potentials ($V_{rev}$) and compare them with the Nernst potentials of potassium ions in various gradients across the membranes (Fig. 7, D and E). To overcome some variations of the currents recorded during the first 200 ms of the activation (80 mV) segments of the pulses, raw data (as exemplified in Fig. S3 B in finer 5-mV steps) were leak-corrected and normalized to the last data point of the activation voltage. The normalization procedure allowed a better comparison of the tail currents (Fig. S3 C). The change of the tail currents from inward to outward was used to recognize the reversal potential, as showed in the magnified view of the tail currents in Fig. S3 C, where the reversal potential was close to 0 mV, agreeing with $E_k$ = 0 mV. As another example, when $E_k$ was set at 40 mV, the measured reversal potential from the KvAP channels in the bSUMs was 38 mV (Fig. 7 D). Under three different solution conditions, we found that the measured reversal potentials closely followed the calculated Nernst potentials for $K^+$ (Fig. 7 E), suggesting that the channel conducts potassium ions with a high degree of selectivity. These data further suggest that the recorded activity in the patches was from KvAP channels in the bSUMs. Even though the kinetics of the channel appeared to be different in the bSUMs, similar to channels in GUVs (Aimon et al., 2011), a detailed kinetic analysis of activation, inactivation, and deactivation will be needed in a separate study.

### bSUMs of varying dimensions and lipid compositions

The cryoEM images of 200-nm bSUMs, the fluorescence images of 5-µm bSUMs, and the electrical recordings from the bSUMs suggest that as long as it is possible to introduce enough proteins onto the surfaces of the beads, bSUMs of even larger diameters can be prepared. We tested the formation of bSUMs around 5-, 10-, and 20-µm silica beads and were able to record voltage-dependent activity from KvAP channels in these bSUMs (Fig. 8, A–C). Similar to what was observed from KvAP in giant unilamellar vesicles, the G-V relation of the KvAP in PE/PG lipids has a shallow component in the high voltage range (Aimon et al., 2011). We therefore showed traces elicited by voltage pulses from 0 to 160 mV at 40-mV steps. These large-sized bSUMs make good candidates for electrical recordings via giant patch methods (Hilgemann and Lu, 1998). Our initial test suggested that it is possible to make recordings from hundreds of thousands of channels. The technical details of making giant patch recordings are being optimized and will be reported separately. When we made KvAP bSUMs with different lipids (Fig. 8, D–F), we were able to record channel activity from PE/PG and DOPC membranes as well as membranes containing a mixture of DOPC/cholesterol (19:1 weight ratio; Fig. 8 F). There were apparent changes because in the cholesterol-containing membranes, the channels only started to show activity when transmembrane potential is >50 mV, which will need to be thoroughly quantified in a separate study.

## DISCUSSION

Our results demonstrate that with chemical modifications (Ni-NTA as an example here) to their surfaces, silica beads (as well as other beads tested in the laboratory) were able to retain a high density of His-tagged channel molecules (Figs. 2 and 3), which act as membrane organization centers during bilayer reconstitution and allow the formation of continuous unilamellar bilayers on the surfaces of individual beads; we named these bSUMs (Figs. 3–5). The relatively uniform orientation of the inserted proteins was achieved via their selective attachment to the surfaces of the beads in detergents. The channel proteins were found to be biochemically intact (Fig. 5). Their basic electrical activity remains similar to what was previously observed in the BLMs (Fig. 7), even though there are obvious differences in the kinetics of activation and inactivation. The bSUM system can be of various dimensions. Given the random incorporation of lipids into the bilayers, specific lipids introduced during membrane reconstitution will very likely dictate the lipid composition of bSUMs. Because of limited materials and the difficulty involved in lipid quantification, we have not been able to accurately determine the lipid composition of our bSUMs. With more development in lipid quantification via mass spectrometry, we expect to be able to directly determine the lipid composition of the bSUMs in the future. Our results demonstrate that the new bSUM method is successful, as we diagramed in Fig. 1. It allows relatively good control over protein orientation and should be suitable for studying lipid-dependent gating effects on voltage-gated ion channels.

The bSUMs embody a high density of membrane proteins that to a large extent favor one direction. Each 20-µm bead retains ∼960,000 molecules, assuming a surface density of 800 per $\mu m^2$ (3,200/4, four His-tags per channel), which is close to what we measured before under EM (Llaguno et al., 2014). If a reliable method of giant-patch recording can be established, we expect to be able to measure gating currents directly from voltage-gated ion channels in bSUMs. 300,000 KvAP channels (one third of the surface area of one 20-µm bead) are expected to generate a gating current of ∼60 pA over a 10-ms period. We expect that the bSUMs will have broader applications concerning various transporter proteins after the successful optimization of the giant patch recordings (Hilgemann and Lu, 1998) or using glass chips with ∼10–20-µm openings.

The reconstitution of a bSUM is likely to be dictated by the hydrophobic transmembrane domains of selectively anchored proteins. After lipids are mixed with the

protein-detergent micelles on the bead surface, detergent removal initiates the gradual enrichment of lipids around the proteins. During the physical growth of membranes from nanometers to micrometers, we speculate that small patches of bilayers will form first, with detergents either inserted in the bilayer portion or forming micelles around the rims of these patches, and that the gradual growth of these patches will be supported by the fusion of small detergent-saturated vesicles (or membrane patches) formed in solution. When membrane patches around neighboring proteins are sizeable enough to touch one another and fuse, a continuous bilayer will come into shape. In addition, small vesicles without proteins are formed in the bulk solvent phase, and residual detergents may be able to mediate the fusion of these small vesicles into the bilayers around individual proteins such that after the complete removal of the detergents, the continuous bilayers will have no leaks or tension.

During membrane reconstitution, many factors, including temperature, rate of detergent removal, ionic strength, pH, etc., may affect bilayer formation (Lee et al., 2013). Our stepwise removal of detergents may control the fusion of small membrane patches around proteins, as well as, in the later phase, the fusion of small vesicles in the solution into the bilayers around the proteins. Because the distribution of lipids into the various phases is random, we expect that without the binding of specific lipids to the membrane proteins, the same lipid composition should be maintained as in the starting lipid mixture. Because of the technical limits involved in quantifying specific lipids, we have not been able to reliably measure the lipid composition of the bSUMs. However, when we purified the KvAP channels, we did not detect any bound lipids via thin-layer chromatography, suggesting that our assumption of the bSUMs having the same lipid composition as the input lipid mixture was likely correct. With more advanced mass spectrometry technology, it will become feasible to quantify each type of lipid and measure lipid composition in bSUMs (Kraft and Klitzing, 2014).

Because the channel proteins on the bead surface appear to be the main factors in reconstituting a unilamellar membrane, we expect that the detergent-solubilized lipids are randomly inserted into the bilayer. This means that introducing the desired lipids during reconstitution would control the lipid composition of the bSUMs. Such easy control of lipid composition relies on the random distribution of lipids in detergent micelles and the lack of phase separation during membrane reconstitution; thus, all lipid molecules in the mixture have an equal probability of being inserted into the bSUMs. Human cell membranes are made of membrane proteins and many types of lipids. Among these lipid molecules, phospholipids, glycolipids, sphingolipids, and cholesterol are the main species. In cell membranes, lipids and proteins are not randomly distributed but instead organized into microdomains, which include lipid rafts and caveolae (Anderson, 1993, 1998; Simons and Ikonen, 2000; Simons and Ehehalt, 2002; Anderson and Blaustein, 2008). How the spatial organization of lipids and membrane proteins affects the function of cell membranes remains a challenging question and has been difficult to study without the capacity to deal with local heterogeneity in an ultramicroscopic scale. The bSUM offers a new method suitable for inserting membrane proteins into bilayers of various lipid compositions and will be useful for studying membrane proteins in bilayers that mimic eukaryotic cell membranes but are usually difficult to prepare using conventional methods.

Even though our current bSUMs are made on spherical beads, the bilayer-forming scheme behind bSUMs is, in principle, applicable to substrates of other shapes. As long as surface engineering allows the selective enrichment of a high density of membrane proteins, it will be feasible to produce supported unilamellar membranes. These supported membranes may be used for other applications, for example, the controlled release of medicinal drugs, and may provide new capacities because of the favored directional insertion of membrane proteins into a single bilayer. For example, heat-resistant bacteriorhodopsin has been engineered and inserted into membranes for bio-solar devices, but the random insertion of the protein into the membrane placed significant limits on its application (Zaitsev et al., 2012). Unidirectional or heavily biased vectorial insertion based on selective enrichment on specific substrates may overcome such a technical barrier.

The limited space underneath the current bSUM places an apparent limit on its potential applications for other purposes. We have tested the potential formation of bSUMs around porous beads. It was successful as long as the pores in the beads were small (e.g., <10 nm). Other possible configurations include the construction of a shell-like support with small pores so that the interior of the beads is largely empty. Supported monolayers formed directly on the surface of porous poly-(lactide-glycolide) beads have been proposed as a drug-delivery vehicle (Musumeci et al., 2006; Hild et al., 2011). The bSUMs on porous beads with specific proteins integrated into the membranes may provide a new vehicle that can be used for controlled and targeted drug release in the future.

The cryoEM images of the 200-nm KvAP-bSUMs suggest that when it is feasible to control the bSUMs in the range of 50–100 nm, it may become suitable to use such bSUMs for molecular imaging. Based on the surface density estimated from our study, there are five to eight channels in each 50-nm bSUM. These molecules are well separated, on average ∼40 nm apart. The favored protein orientation and the spherical shape of the

beads make these miniaturized bSUMs suitable for cryoEM imaging. With beads that are porous and have a physical density close to that of water, the images from miniaturized bSUMs will be useful for spherically constrained reconstruction (Jiang et al., 2001; Wang and Sigworth, 2009), a method capable of obtaining 3-D structures of membrane proteins in membrane by single-particle reconstruction. Future studies will test the feasibility of this new imaging modality.

We thank Dr. Michael X. Zhu at UT Health Science Center at Houston for providing access to his Nanion Port-a-Patch system in the early stage of this project and for valuable discussions regarding the fabrication and applications of bSUMs and his comments on the manuscript. Dr. William Snell (UT Southwestern Medical Center) offered insights on the potential applications of the bSUMs to other membrane proteins and membrane processes inside a cell. Dr. Donald Hilgemann (UT Southwestern Medical Center) provided valuable technical advice and evaluated the possible recordings from bSUMs using giant-patch electrodes. Drs. Hilgemann and Paul Blount at UT Southwestern Medical Center and Dr. Christopher Miller at Brandeis University offered valuable comments on the manuscript.

This work was supported by an American Heart Association National Innovative Award (12IRG9400019 to Q.-X. Jiang), a National Institutes of Health (NIH) grant (R01GM093271 to Q.-X. Jiang), and an NIGMS EUREKA award (R01GM088745 to Q.-X. Jiang). Q.-X. Jiang was also supported by the Welch Foundation (I-1684) and CPRIT (RP120474). The K2 Summit Direct Detector and the Gatan XP1 UltraScan CCD camera used for cryoEM imaging were purchased with the support of a Shared Instrument Grant from NIH (S10RR027972 to Q.-X. Jiang). This work was partly performed in laboratories constructed with support from NIH (grant C06RR30414 with Dr. Jerry Shay as the principal investigator).

The authors declare no competing financial interests.

Author contributions: Q.-X. Jiang conceived the design of the experiments and oversaw all steps of the implementation of the bSUMs. S. Lee and H. Zheng performed all the experiments. M.C. Llaguno developed the surface engineering procedure and microscopy. All authors contributed to the preparation of the manuscript.

Sharona E. Gordon served as editor.

Submitted: 27 May 2015
Accepted: 7 December 2015

## REFERENCES

Abi-Char, J., A. Maguy, A. Coulombe, E. Balse, P. Ratajczak, J.L. Samuel, S. Nattel, and S.N. Hatem. 2007. Membrane cholesterol modulates Kv1.5 potassium channel distribution and function in rat cardiomyocytes. *J. Physiol.* 582:1205–1217. http://dx.doi.org/10.1113/jphysiol.2007.134809

Aimon, S., J. Manzi, D. Schmidt, J.A. Poveda Larrosa, P. Bassereau, and G.E. Toombes. 2011. Functional reconstitution of a voltage-gated potassium channel in giant unilamellar vesicles. *PLoS One.* 6:e25529. http://dx.doi.org/10.1371/journal.pone.0025529

Anderson, R.G. 1993. Caveolae: where incoming and outgoing messengers meet. *Proc. Natl. Acad. Sci. USA.* 90:10909–10913. http://dx.doi.org/10.1073/pnas.90.23.10909

Anderson, R.G. 1998. The caveolae membrane system. *Annu. Rev. Biochem.* 67:199–225. http://dx.doi.org/10.1146/annurev.biochem.67.1.199

Anderson, D.S., and R.O. Blaustein. 2008. Preventing voltage-dependent gating of anthrax toxin channels using engineered disulfides. *J. Gen. Physiol.* 132:351–360. http://dx.doi.org/10.1085/jgp.200809984

Atanasov, V., N. Knorr, R.S. Duran, S. Ingebrandt, A. Offenhäusser, W. Knoll, and I. Köper. 2005. Membrane on a chip: A functional tethered lipid bilayer membrane on silicon oxide surfaces. *Biophys. J.* 89:1780–1788. http://dx.doi.org/10.1529/biophysj.105.061374

Bayley, H., B. Cronin, A. Heron, M.A. Holden, W.L. Hwang, R. Syeda, J. Thompson, and M. Wallace. 2008. Droplet interface bilayers. *Mol. Biosyst.* 4:1191–1208. http://dx.doi.org/10.1039/b808893d

Bezanilla, F. 2008. How membrane proteins sense voltage. *Nat. Rev. Mol. Cell Biol.* 9:323–332. http://dx.doi.org/10.1038/nrm2376

Brohawn, S.G., Z. Su, and R. MacKinnon. 2014. Mechanosensitivity is mediated directly by the lipid membrane in TRAAK and TREK1 $K^+$ channels. *Proc. Natl. Acad. Sci. USA.* 111:3614–3619. http://dx.doi.org/10.1073/pnas.1320768111

Catterall, W.A. 2012. Voltage-gated sodium channels at 60: structure, function and pathophysiology. *J. Physiol.* 590:2577–2589. http://dx.doi.org/10.1113/jphysiol.2011.224204

Catterall, W.A., and V. Yarov-Yarovoy. 2010. Helical motion of an S4 voltage sensor revealed by gating pore currents. *Channels (Austin).* 4:75–77. http://dx.doi.org/10.4161/chan.4.2.10998

Chun, Y.S., S. Shin, Y. Kim, H. Cho, M.K. Park, T.W. Kim, S.V. Voronov, G. Di Paolo, B.C. Suh, and S. Chung. 2010. Cholesterol modulates ion channels via down-regulation of phosphatidylinositol 4,5-bisphosphate. *J. Neurochem.* 112:1286–1294. http://dx.doi.org/10.1111/j.1471-4159.2009.06545.x

Chun, Y.S., H.G. Oh, M.K. Park, H. Cho, and S. Chung. 2013. Cholesterol regulates HERG $K^+$ channel activation by increasing phospholipase C β1 expression. *Channels (Austin).* 7:275–287. http://dx.doi.org/10.4161/chan.25122

Cohen, F.S., M.H. Akabas, J. Zimmerberg, and A. Finkelstein. 1984. Parameters affecting the fusion of unilamellar phospholipid vesicles with planar bilayer membranes. *J. Cell Biol.* 98:1054–1062. http://dx.doi.org/10.1083/jcb.98.3.1054

Coyan, F.C., F. Abderemane-Ali, M.Y. Amarouch, J. Piron, J. Mordel, C.S. Nicolas, M. Steenman, J. Mérot, C. Marionneau, A. Thomas, et al. 2014. A long QT mutation substitutes cholesterol for phosphatidylinositol-4,5-bisphosphate in KCNQ1 channel regulation. *PLoS One.* 9:e93255. http://dx.doi.org/10.1371/journal.pone.0093255

DeCaen, P.G., V. Yarov-Yarovoy, T. Scheuer, and W.A. Catterall. 2011. Gating charge interactions with the S1 segment during activation of a $Na^+$ channel voltage sensor. *Proc. Natl. Acad. Sci. USA.* 108:18825–18830. http://dx.doi.org/10.1073/pnas.1116449108

Finol-Urdaneta, R.K., J.R. McArthur, P.F. Juranka, R.J. French, and C.E. Morris. 2010. Modulation of KvAP unitary conductance and gating by 1-alkanols and other surface active agents. *Biophys. J.* 98:762–772. http://dx.doi.org/10.1016/j.bpj.2009.10.053

Gaffield, M.A., S.O. Rizzoli, and W.J. Betz. 2006. Mobility of synaptic vesicles in different pools in resting and stimulated frog motor nerve terminals. *Neuron.* 51:317–325. http://dx.doi.org/10.1016/j.neuron.2006.06.031

Guo, J., S. Chi, H. Xu, G. Jin, and Z. Qi. 2008. Effects of cholesterol levels on the excitability of rat hippocampal neurons. *Mol. Membr. Biol.* 25:216–223. http://dx.doi.org/10.1080/09687680701805541

Hajdú, P., Z. Varga, C. Pieri, G. Panyi, and R. Gáspár Jr. 2003. Cholesterol modifies the gating of Kv1.3 in human T lymphocytes. *Pflugers Arch.* 445:674–682. http://dx.doi.org/10.1007/s00424-002-0974-y

Hild, N., O.D. Schneider, D. Mohn, N.A. Luechinger, F.M. Koehler, S. Hofmann, J.R. Vetsch, B.W. Thimm, R. Müller, and W.J. Stark. 2011. Two-layer membranes of calcium phosphate/collagen/

PLGA nanofibres: in vitro biomineralisation and osteogenic differentiation of human mesenchymal stem cells. *Nanoscale.* 3:401–409. http://dx.doi.org/10.1039/C0NR00615G

Hilgemann, D.W., and C.C. Lu. 1998. Giant membrane patches: Improvements and applications. *Methods Enzymol.* 293:267–280. http://dx.doi.org/10.1016/S0076-6879(98)93018-X

Hite, R.K., J.A. Butterwick, and R. MacKinnon. 2014. Phosphatidic acid modulation of Kv channel voltage sensor function. *eLife.* 3:04366. http://dx.doi.org/10.7554/eLife.04366

Iscla, I., R. Wray, and P. Blount. 2011. An in vivo screen reveals protein-lipid interactions crucial for gating a mechanosensitive channel. *FASEB J.* 25:694–702. http://dx.doi.org/10.1096/fj.10-170878

Jiang, Q.-X., and T. Gonen. 2012. The influence of lipids on voltage-gated ion channels. *Curr. Opin. Struct. Biol.* 22:529–536. http://dx.doi.org/10.1016/j.sbi.2012.03.009

Jiang, Q.-X., D.W. Chester, and F.J. Sigworth. 2001. Spherical reconstruction: A method for structure determination of membrane proteins from cryo-EM images. *J. Struct. Biol.* 133:119–131. http://dx.doi.org/10.1006/jsbi.2001.4376

Jiang, Q.-X., D.N. Wang, and R. MacKinnon. 2004. Electron microscopic analysis of KvAP voltage-dependent $K^+$ channels in an open conformation. *Nature.* 430:806–810. http://dx.doi.org/10.1038/nature02735

Jiang, Y., V. Ruta, J. Chen, A. Lee, and R. MacKinnon. 2003. The principle of gating charge movement in a voltage-dependent $K^+$ channel. *Nature.* 423:42–48. http://dx.doi.org/10.1038/nature01581

Kraft, M.L., and H.A. Klitzing. 2014. Imaging lipids with secondary ion mass spectrometry. *Biochim. Biophys. Acta.* 1841:1108–1119. http://dx.doi.org/10.1016/j.bbalip.2014.03.003

Lee, S., H. Zheng, L. Shi, and Q.X. Jiang. 2013. Reconstitution of a Kv channel into lipid membranes for structural and functional studies. *J. Vis. Exp.* 77:e50436. http://dx.doi.org/10.3791/50436

Lewis, B.A., and D.M. Engelman. 1983. Lipid bilayer thickness varies linearly with acyl chain length in fluid phosphatidylcholine vesicles. *J. Mol. Biol.* 166:211–217. http://dx.doi.org/10.1016/S0022-2836(83)80007-2

Llaguno, M.C., H. Xu, L. Shi, N. Huang, H. Zhang, Q. Liu, and Q.X. Jiang. 2014. Chemically functionalized carbon films for single molecule imaging. *J. Struct. Biol.* 185:405–417. http://dx.doi.org/10.1016/j.jsb.2014.01.006

Long, S.B., X. Tao, E.B. Campbell, and R. MacKinnon. 2007. Atomic structure of a voltage-dependent $K^+$ channel in a lipid membrane-like environment. *Nature.* 450:376–382. http://dx.doi.org/10.1038/nature06265

MacKinnon, R. 2003. Potassium channels. *FEBS Lett.* 555:62–65. http://dx.doi.org/10.1016/S0014-5793(03)01104-9

Martens, J.R., R. Navarro-Polanco, E.A. Coppock, A. Nishiyama, L. Parshley, T.D. Grobaski, and M.M. Tamkun. 2000. Differential targeting of Shaker-like potassium channels to lipid rafts. *J. Biol. Chem.* 275:7443–7446. http://dx.doi.org/10.1074/jbc.275.11.7443

Martens, J.R., K. O'Connell, and M. Tamkun. 2004. Targeting of ion channels to membrane microdomains: localization of $K_V$ channels to lipid rafts. *Trends Pharmacol. Sci.* 25:16–21. http://dx.doi.org/10.1016/j.tips.2003.11.007

Miller, C. 2003. A charged view of voltage-gated ion channels. *Nat. Struct. Biol.* 10:422–424. http://dx.doi.org/10.1038/nsb0603-422

Musumeci, T., C.A. Ventura, I. Giannone, B. Ruozi, L. Montenegro, R. Pignatello, and G. Puglisi. 2006. PLA/PLGA nanoparticles for sustained release of docetaxel. *Int. J. Pharm.* 325:172–179. http://dx.doi.org/10.1016/j.ijpharm.2006.06.023

Needham, D., T.J. McIntosh, and E. Evans. 1988. Thermomechanical and transition properties of dimyristoylphosphatidylcholine/cholesterol bilayers. *Biochemistry.* 27:4668–4673. http://dx.doi.org/10.1021/bi00413a013

Payandeh, J., T. Scheuer, N. Zheng, and W.A. Catterall. 2011. The crystal structure of a voltage-gated sodium channel. *Nature.* 475:353–358. http://dx.doi.org/10.1038/nature10238

Payandeh, J., T.M. Gamal El-Din, T. Scheuer, N. Zheng, and W.A. Catterall. 2012. Crystal structure of a voltage-gated sodium channel in two potentially inactivated states. *Nature.* 486:135–139.

Piasta, K.N., D.L. Theobald, and C. Miller. 2011. Potassium-selective block of barium permeation through single KcsA channels. *J. Gen. Physiol.* 138:421–436. http://dx.doi.org/10.1085/jgp.201110684

Pristerà, A., M.D. Baker, and K. Okuse. 2012. Association between tetrodotoxin resistant channels and lipid rafts regulates sensory neuron excitability. *PLoS One.* 7:e40079. http://dx.doi.org/10.1371/journal.pone.0040079

Ramu, Y., Y. Xu, and Z. Lu. 2006. Enzymatic activation of voltage-gated potassium channels. *Nature.* 442:696–699. http://dx.doi.org/10.1038/nature04880

Ruta, V., Y. Jiang, A. Lee, J. Chen, and R. MacKinnon. 2003. Functional analysis of an archaebacterial voltage-dependent $K^+$ channel. *Nature.* 422:180–185. http://dx.doi.org/10.1038/nature01473

Saini, H.K., A.S. Arneja, and N.S. Dhalla. 2004. Role of cholesterol in cardiovascular dysfunction. *Can. J. Cardiol.* 20:333–346.

Schmidt, D., and R. MacKinnon. 2008. Voltage-dependent $K^+$ channel gating and voltage sensor toxin sensitivity depend on the mechanical state of the lipid membrane. *Proc. Natl. Acad. Sci. USA.* 105:19276–19281. http://dx.doi.org/10.1073/pnas.0810187105

Schmidt, D., Q.X. Jiang, and R. MacKinnon. 2006. Phospholipids and the origin of cationic gating charges in voltage sensors. *Nature.* 444:775–779. http://dx.doi.org/10.1038/nature05416

Schulz, P., B. Dueck, A. Mourot, L. Hatahet, and K. Fendler. 2009. Measuring ion channels on solid supported membranes. *Biophys. J.* 97:388–396. http://dx.doi.org/10.1016/j.bpj.2009.04.022

Simons, K., and R. Ehehalt. 2002. Cholesterol, lipid rafts, and disease. *J. Clin. Invest.* 110:597–603. http://dx.doi.org/10.1172/JCI0216390

Simons, K., and E. Ikonen. 2000. How cells handle cholesterol. *Science.* 290:1721–1726. http://dx.doi.org/10.1126/science.290.5497.1721

Tao, X., A. Lee, W. Limapichat, D.A. Dougherty, and R. MacKinnon. 2010. A gating charge transfer center in voltage sensors. *Science.* 328:67–73. http://dx.doi.org/10.1126/science.1185954

Tombola, F., M.M. Pathak, and E.Y. Isacoff. 2006. How does voltage open an ion channel? *Annu. Rev. Cell Dev. Biol.* 22:23–52. http://dx.doi.org/10.1146/annurev.cellbio.21.020404.145837

Tombola, F., M.M. Pathak, P. Gorostiza, and E.Y. Isacoff. 2007. The twisted ion-permeation pathway of a resting voltage-sensing domain. *Nature.* 445:546–549. http://dx.doi.org/10.1038/nature05396

Tóth, A., O. Szilágyi, Z. Krasznai, G. Panyi, and P. Hajdú. 2009. Functional consequences of Kv1.3 ion channel rearrangement into the immunological synapse. *Immunol. Lett.* 125:15–21. http://dx.doi.org/10.1016/j.imlet.2009.05.004

Vargas, E., F. Bezanilla, and B. Roux. 2011. In search of a consensus model of the resting state of a voltage-sensing domain. *Neuron.* 72:713–720. http://dx.doi.org/10.1016/j.neuron.2011.09.024

Villalba-Galea, C.A., F. Miceli, M. Taglialatela, and F. Bezanilla. 2009a. Coupling between the voltage-sensing and phosphatase domains of Ci-VSP. *J. Gen. Physiol.* 134:5–14. http://dx.doi.org/10.1085/jgp.200910215

Villalba-Galea, C.A., W. Sandtner, D. Dimitrov, H. Mutoh, T. Knöpfel, and F. Bezanilla. 2009b. Charge movement of a voltage-sensitive fluorescent protein. *Biophys. J.* 96:L19–L21. http://dx.doi.org/10.1016/j.bpj.2008.11.003

Wang, D., and B.G. Schreurs. 2010. Dietary cholesterol modulates the excitability of rabbit hippocampal CA1 pyramidal neurons. *Neurosci. Lett.* 479:327–331. http://dx.doi.org/10.1016/j.neulet.2010.05.090

Wang, L., and F.J. Sigworth. 2009. Structure of the BK potassium channel in a lipid membrane from electron cryomicroscopy. *Nature*. 461:292–295. http://dx.doi.org/10.1038/nature08291

Xia, F., X. Gao, E. Kwan, P.P. Lam, L. Chan, K. Sy, L. Sheu, M.B. Wheeler, H.Y. Gaisano, and R.G. Tsushima. 2004. Disruption of pancreatic beta-cell lipid rafts modifies Kv2.1 channel gating and insulin exocytosis. *J. Biol. Chem.* 279:24685–24691. http://dx.doi.org/10.1074/jbc.M314314200

Xia, F., L. Xie, A. Mihic, X. Gao, Y. Chen, H.Y. Gaisano, and R.G. Tsushima. 2008. Inhibition of cholesterol biosynthesis impairs insulin secretion and voltage-gated calcium channel function in pancreatic beta-cells. *Endocrinology*. 149:5136–5145. http://dx.doi.org/10.1210/en.2008-0161

Xu, Y., Y. Ramu, and Z. Lu. 2008. Removal of phospho-head groups of membrane lipids immobilizes voltage sensors of $K^+$ channels. *Nature*. 451:826–829. http://dx.doi.org/10.1038/nature06618

Yang, Y., Y. Yan, and F.J. Sigworth. 2004. Can Shaker potassium channels be locked in the deactivated state? *J. Gen. Physiol.* 124:163–171. http://dx.doi.org/10.1085/jgp.200409057

Zaitsev, S.Y., D.O. Solovyeva, and I. Nabiev. 2012. Thin films and assemblies of photosensitive membrane proteins and colloidal nanocrystals for engineering of hybrid materials with advanced properties. *Adv. Colloid Interface Sci.* 183–184:14–29. http://dx.doi.org/10.1016/j.cis.2012.07.003

Zaydman, M.A., and J. Cui. 2014. PIP2 regulation of KCNQ channels: biophysical and molecular mechanisms for lipid modulation of voltage-dependent gating. *Front. Physiol.* 5:195. http://dx.doi.org/10.3389/fphys.2014.00195

Zaydman, M.A., J.R. Silva, K. Delaloye, Y. Li, H. Liang, H.P. Larsson, J. Shi, and J. Cui. 2013. Kv7.1 ion channels require a lipid to couple voltage sensing to pore opening. *Proc. Natl. Acad. Sci. USA*. 110:13180–13185. http://dx.doi.org/10.1073/pnas.1305167110

Zaydman, M.A., M.A. Kasimova, K. McFarland, Z. Beller, P. Hou, H.E. Kinser, H. Liang, G. Zhang, J. Shi, M. Tarek, and J. Cui. 2014. Domain-domain interactions determine the gating, permeation, pharmacology, and subunit modulation of the IKs ion channel. *eLife*. 3:e03606. http://dx.doi.org/10.7554/eLife.03606

Zheng, H., W. Liu, L.Y. Anderson, and Q.X. Jiang. 2011. Lipid-dependent gating of a voltage-gated potassium channel. *Nat. Commun.* 2:250. http://dx.doi.org/10.1038/ncomms1254